International Journal of Fluid Power, 2014
Vol. 15, No. 2, 101–111, http://dx.doi.org/10.1080/14399776.2014.931133

Dynamic Model of a Pneumatic Automatic People Mover (Aeromovel System)

João F.F.H. Britto[a]*, Eduardo A. Perondi[b]* and Mário R. Sobczyk S.[b]*

[a]*E&P Production Development Projects – Artificial Lift and Subsea Dept. – Petróleo Brasileiro S.A. Rio de Janeiro – RJ – Brazil;* [b]*Dept. of Mechanical Engineering, Universidade Federal do Rio Grande do Sul, Porto Alegre – RS – Brazil*

This paper presents a new mathematical model for the Aeromovel transport system, which is a non-conventional Automated People Mover (APM) based on pneumatics. The vehicle runs over rails installed on an elevated guide, being propelled by air that is pressurised by means of an external power source (a blower) installed on the ground. The proposed lumped-parameter model is intended as an auxiliary tool for the development of this technology, especially in what concerns its trajectory control algorithms. The dynamics of the pressures in the chambers of the actuation pipe are modelled with basis on energy and continuity assumptions, and important phenomena, such as air compressibility, leakages, and steady-state head losses, are taken into account. The model is validated by the comparison between results of simulations and direct measurements performed in a real-scale prototype constructed in Porto Alegre, Brazil.

Keywords: dynamic models, pneumatics, Aeromovel transport system, Automated People Mover

1. Introduction

1.1. Background

Aeromovel is a transport system whose vehicle travels on suspended rails, differing from other Automated People Movers (APM) by using pneumatic propulsion. It is currently being studied as an alternative way to reduce traffic problems in urban centres. The first line available for public use was installed in an amusement park in Jakarta, Indonesia, and a commercial line, connecting the airport of Porto Alegre, Brazil, to an urban train surface line is now being constructed (Aeromovel, 2013). Movement is caused by blowers fixed to the ground, which allow the air to be blown to (or relieved from) the interior of a pipe constructed inside the guide structure, pushing (or pulling) the vehicle. Thus, because it does not need to carry its own engine, the dead weight of the vehicle and its associated energy consumption are significantly reduced, which also allows the structures that support the rails to be lighter, diminishing the construction costs.

The main elements of the system are illustrated in Figure 1. Each vehicle has two internal pistons that divide the pipe inside of the guide in three chambers, so that pressure differences can be generated in order to make the vehicle move. The connections of the vehicle to the line pistons are similar to that of a rodless pneumatic cylinder: the line has a rectangular slot running along its entire length, and thin bars passing through the rubber-bladed seals link the pistons to the vehicle. As the vehicle runs forward, these bars open a gap between the seal blades, which close again as the vehicle moves on. Still in Figure 1, two types of valves are highlighted: the atmospheric valves (V_a), which connect the chambers to the atmosphere; and the power valves (V_p), which regulate the air mass flow rates $\dot{m}_1$ and $\dot{m}_2$ into and out of each pipe chamber, so that the dynamics of the pressures that drive the vehicle can be controlled. The Power Propulsion Unit (PPU) consists of a centrifugal fan with its electric driving system and a group of four flow-directional valves. The metallic wheels of the vehicle are distributed in independent sets of four elements (*trucks*). Each wheel holds a disk brake equipped with an anti-lock braking system (ABS). A basic Aeromovel module is denominated *standard block*, consisting basically of one vehicle, two PPUs, and one pair of V_a and another of V_p valves. With this configuration, three operation modes are possible:

Push: assuming that the movement occurs from Station 1 to Station 2, the vehicle is pushed by the pressurised air provided by the PPU to its upstream side (PPU_1) where the atmospheric valve V_{a1} is closed. Meanwhile, to the downstream side of the pipe, the atmospheric valve V_{a2} next to PPU_2 remains open. The air flow into the line is regulated by the proportional valve V_{p1}.

Pull: maintaining upstream V_{a1} valve open, the air is exhausted by the PPU_2 unit, causing a pressure drop in the pipe section to the downstream side of the vehicle. In this case, V_{a2} is kept closed and the exhausted air flow is regulated by means of V_{p2}.

Push–Pull: the vehicle is simultaneously pushed by the PPU on the upstream side and pulled by the other PPU on the downstream side of the duct.

The operation principle is very similar to that of a regular pneumatic actuator (see, e.g., Virvalo and Koskinen, 1988; Maré et al., 2000). A typical shuttle trip under *Push* operation mode can be described as follows:

*Corresponding authors. Email: mario.sobczyk@ufrgs.br (J.F.F.H. Britto); jf.1.fhb@gmail.com (E.A. Perondi); eduardo.perondi@ufrgs.br (M.R. Sobczyk S.)

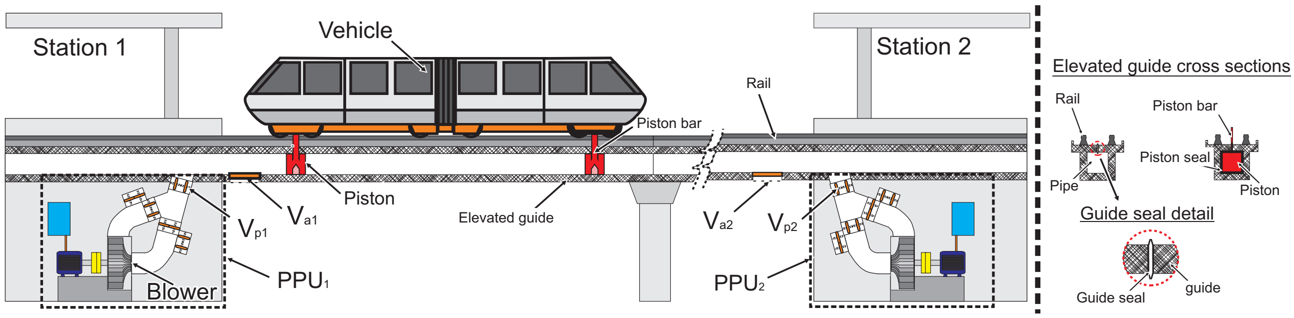

Figure 1. Aeromovel operation principle and main elements.

when the vehicle moves from station 1 to station 2, chamber 1 is pressurised by the air that flows from PPU_1 through V_{p1}. Meanwhile, chamber 2 is connected to the atmosphere by means of V_{a2}. As a result, a difference in pressure between both chambers is established, causing the vehicle to move in the desired direction. The direction of the movement can be reversed by inverting the valves' configuration. When the combination of the valves is suitably changed, the system operation in the *Pull* and *Push–Pull* modes can be described in similar terms.

1.2. *Problem statement*

Compared to other transport systems, Aeromovel is a relatively new technology. Thus, in order to bring it to a fully developed stage, it is still necessary to analyse many aspects of its operation characteristics. An adequate mathematical model of the system may be of great utility in this process, for it allows different configurations to be evaluated quickly, easily, and at low cost.

The models of the Aeromovel system currently found in the bibliography are based on rather idealised assumptions, where important phenomena such as leakages and the compressibility of air are neglected. In actual plants, however, distances between PPUs and the vehicle can be of 500 m or more, and as the cross-sectional area is about 1 m^2, high volumes (500 m^3 or more) have to be filled or exhausted to establish the necessary pressures to drive the vehicle appropriately, resulting in a significant delay that must be taken into account in trajectory control problems, for instance. These facts indicate that existing models of the Aeromovel system fail to represent important characteristics of the actual plant for control applications. On the other hand, because one of the main purposes of this model lies in the development of control algorithms, such model must be analytically tractable, so that stability issues and other dynamic properties of the real system can be addressed in a straightforward manner. Therefore, its mathematical structure must be relatively simple, even if non-linear, and it must be of low dynamic order. In the light of such observations, the main contributions of this paper can be summarised as the proposition and experimental validation of a low-order, lumped-parameter mathematical model for the Aeromovel technology, taking into account phenomena that affect its performance and which have not been considered in previous works, such as:

- air compressibility;
- wheels–rail contact friction forces (allowing the simulation of braking conditions);
- fan blower behaviour;
- air leakages; and
- gravity effects due to hill acclivities along the line.

The present paper is organised as follows. Section 2 is dedicated to the related work description. The vehicle and power system modelling are presented in Section 3. The experimental test line is depicted in Section 4, and the model evaluation is carried out in Section 5. Finally, the conclusions are outlined in Section 6.

2. Related work

There are few references in the literature about Aeromovel technology. The first works about its modelling mainly focused on its energetic efficiency analysis, and all of them assumed incompressible air characteristics. When the system was first proposed, Ferreira and Sadhu (1981) employed a simplified model for deciding favourably on supporting the construction of an experimental line to study the viability of the then-novel technology. This result was opposed by Costa (1981), also based on a plain model, which concluded that the system's energy consumption would be about six times larger than that of traditional transport means. In spite of such opposition, the experimental line was built between 1981 and 1987.

The so-called *Pilot Line* was studied in Ferreira (1984), where pressure, velocity, and electrical energy consumption data were acquired, aimed at analysing the energetic efficiency of the Aeromovel system. It was concluded that Aeromovel would be viable compared with other equivalent means of transport. More recently, with the growth of transportation problems worldwide and with the emphasis on "clean" technologies, Aeromovel is once again being considered as an attractive alternative for urban transport systems. Accordingly, its study in technical-oriented papers is also being renewed.

More recently, Boulter (1999) presented a linear mathematical model of Aeromovel, which was used in the development of a trajectory tracking controller. Based on theoretical results, the author concluded that it would be possible to control the vehicle trajectory by varying the angular velocity of the fan. Freitag and Detoni (2000) deal with the braking control of the system by developing a linear Proportional Integral Derivative (PID) algorithm. The proposed strategy achieved precise responses for fixed loads, but, in the presence of mass variations, the performance deteriorated significantly. To improve robustness to varying loads, Sarmanho et al. (2011) developed an adaptive algorithm based on a recursive mass estimator associated with a gain-schedule control scheme. The results showed that in the empty and full-load cases, the stopping precision was improved from about 0.5 m (fixed control case) to 0.05 m (adaptive control case).

In Sobczyk et al. (2008a, 2008b), a nonlinear cascade control scheme used with success in small-scale pneumatic servopositioners (Perondi and Guenther, 2000) was modified for application to the trajectory tracking control of the Aeromovel vehicle by regulating the proportional aperture of the V_p valves. Simulation results indicated that very satisfactory performances could be achieved with this approach. More recently, Kunz et al. (2011a, 2011b) proposed a timed automata model for the discrete-event part of the Aeromovel control system, so that its algorithm complies with the IEC 61850 communication standards. The authors concluded that the proposed strategy can be applied to the Aeromovel control system synthesis and, by extension, to other APM technologies.

In the next section, the system modelling is developed.

3. Mathematical model

The proposed model is based on a lumped parameters approach. The coordinates and the main variables upon which its development is based are illustrated in Figure 2, and their respective meanings are defined as they appear in the corresponding equations throughout this section. For the sake of study organisation, the system is arbitrarily divided into three smaller subsystems: vehicle, pneumatic chambers, and PPU. The study of each subsystem is presented in the following subsections.

3.1. Vehicle subsystem

Applying Newton's Second Law along the direction of the x-coordinate (distance to the station 1) yields:

$$\begin{aligned} m_{vehic}\ddot{x} &= A_{al}(p_{1al} - p_{2al}) - (F_{seal} + B_{seal}\dot{x}) \\ &\quad - \frac{1}{2}c_D A_{eq}\rho(v_{air} + \dot{x})^2 - F_{adh} - F_{ext} \\ &\quad - m_{vehic} g \sin\varphi_z(x) \end{aligned} \tag{1}$$

where F_{ext} is a generic external force; m_{vehic} is the vehicle mass; A_{al} is the piston area; p_{1al} and p_{2al} are, respectively, downstream and upstream pressures related to the piston surfaces; F_{seal} and B_{seal} are, respectively, the Coulomb friction force and the Newton friction coefficient associated with the piston; v_{air} is the relative air velocity; c_D and A_{eq} are, respectively, the drag coefficient and equivalent area of the transversal section of the vehicle; ρ is the air density; F_{adh} models the wheel–rail adhesion forces; g is the gravity acceleration; and ϕ_z is the slope angle of the line.

The wheel–rail contact forces, F_{adh}, are modelled by considering the Hertz contact theory for elastic bodies, as described in more detail in Polach (2005). This approach is based on the premise that the tangential stress τ_{adh} in the adhesion region presents a crescent linear behaviour up to a maximum value given by $\tau_{adh\max} = \mu\sigma_{\max}$, where μ is a wheel–rail friction coefficient and $\sigma_{\max}$ is the maximum normal stress. In the slip part of the contact region, which has an elliptic shape, τ_{adh} is assumed to be proportional to the normal stress σ. The adhesion force F_{adh} can therefore be obtained by integrating τ_{adh} along the surface of the contact region, which results in:

$$F_{adh} = \frac{2W_{wl}\mu}{\pi}\left(\arctan(\varepsilon) + \frac{\varepsilon}{1+\varepsilon^2}\right) \tag{2}$$

where W_{wl} is the load on the wheel and ε is the gradient of tangential stress in the adhesion region, expressed as:

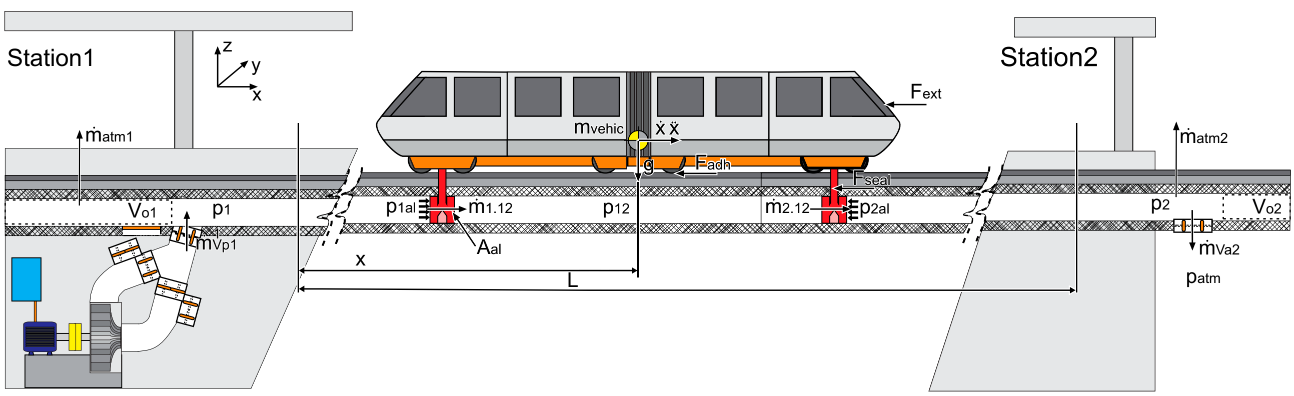

Figure 2. Definition of the main variables.

$$\varepsilon = \frac{1}{4}\frac{G\pi abc_{11}}{W_{wl}\mu}Slip \tag{3}$$

where G is the shear module of the material, a and b are the half-axes of the elliptic contact region, c_{11} is a fixed coefficient given by the linear theory of Kalker (1982) and *Slip* is the creep in the longitudinal direction, given by:

$$Slip = \frac{\dot{x} - \omega_{wl}r_{wl}}{\text{abs}(\max(\dot{x}, \omega_{wl}r_{wl}))} \tag{4}$$

where r_{wl} is the wheel effective radius and the angular velocity ω_{wl}, necessary to calculate the corresponding creep for each wheel (Eq. 4), can be obtained by means of their dynamic equilibrium condition (see Figure 3), which can be expressed as:

$$J_{wh}\dot{\omega}_{wl} = \Gamma_{br} + c_{wh}\omega_{wl} + \Gamma_{wh} - F_{adh}r_{wh} \tag{5}$$

where c_{wh} is the angular friction viscous coefficient; r_{wh} and J_{wh} are, respectively, the wheel radius and moment of inertia; and Γ_{wh} is the external torque.

The braking torque Γ_{br} can be expressed by Eq. 6:

$$\Gamma_{br} = F_{br}r_{br} = (\mu_{discE} + \mu_{discV}\omega_{wl})A_{br}p_{br}r_{br} \tag{6}$$

where μ_{discE} and μ_{discV} are, respectively, Coulomb and kinetic friction coefficients between the disk and the brake pad; A_{br} and r_{br} are, respectively, the area of the hydraulic piston calliper and the calliper average radius; and p_{br} is the hydraulic pressure applied by the brake piston. This system is studied in more detail in Sarmanho et al. (2011).

When the vehicle moves along a curved section of the line, the lateral part of the wheels makes contact with the internal part of the rail. Therefore, the friction effects associated to this contact result in forces contrary to the movement that depend on the mass and velocity of the vehicle and on the radius of the curve. This effect is taken into account as an external force F_{ext} in Eq. 1, given by the centripetal force F_{centr} multiplied by the wheel–rail friction force coefficient μ:

$$F_{ext} = F_{centr}\mu = m_{vehic}\frac{\dot{x}^2}{r_{cv}(x)}\mu \tag{7}$$

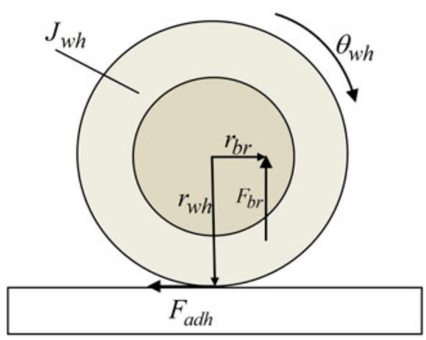

Figure 3. Force balance on a truck wheel.

where $r_{cv}(x)$ is the line curvature radius, which is dependent on the position x of the vehicle.

3.2. Chamber subsystem

In this section, the mathematical description of the dynamics of the pressures in the chambers is provided. The following equations refer to the control volumes relative to the line chambers, as presented in Figure 4.

The analysis is accomplished by means of energy conservation arguments and of considerations about the continuity of the air mass flow. For the control volumes depicted in Figure 4, the principle of energy conservation (Fox and McDonald, 2006) can be expressed as:

$$\begin{cases} \frac{dE}{dt} = \frac{\partial}{\partial t}\int_{V_C} e\rho dV + \int_{Sc} e\rho\vec{\dot{x}}d\vec{A} \\ e = u_i + \frac{\dot{x}^2}{2} + gz \end{cases} \tag{8}$$

where E is the energy in the control volume; e is the specific energy; ρ is the fluid density; V is volume; V_c is the control volume; S_c is the control surface; A is the pipe transverse section area; u_i is the specific internal energy; g is the gravity acceleration; and z is the height from a reference level. The air is regarded as an ideal gas. By integrating with respect to a three-dimensional dominium and using the thermodynamic relations between the specific heats of air, Eq. (8) can be rewritten as:

$$\dot{Q} - p_1\dot{V} = \frac{c_v}{R}\left(V\frac{dp_1}{dt} + p_1\frac{dV}{dt}\right) - c_pT\dot{m}_1 \tag{9}$$

where $\dot{Q}$ is the heat transfer rate; p_1 is the pressure in the upstream control volume; $\dot{V}$ is the volumetric flow rate; R is the particular gas constant; T is the temperature; and $\dot{m}_1$ is the mass flow rate. The total volume of chamber 1 is given by $V_1 = Ax + V_{o1}$, where V_{o1} and $\dot{V}_1 = A\dot{x}$ are the initial volume and the volumetric time rate of the

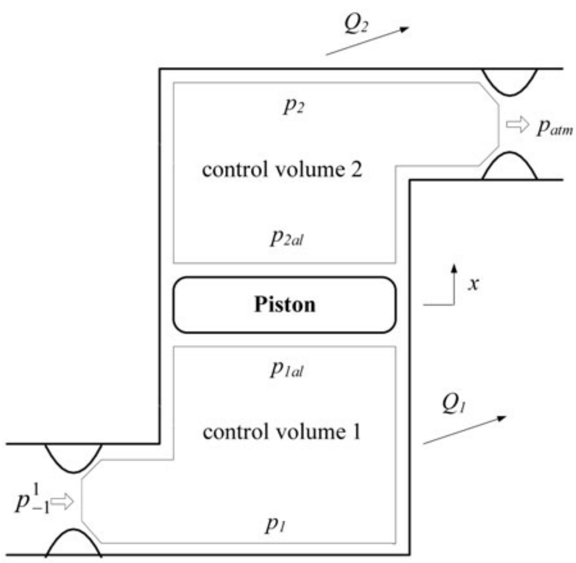

Figure 4. Control volumes for push case.

chamber, respectively. Thus, naming the constant pressure and volume specific heat coefficients ratio (c_p/c_v) as k, Eq. 9 can be rearranged to yield:

$$\frac{dp_1}{dt} = -\frac{p_1 kA}{V_{o1}+Ax}\dot{x} + \frac{RkT}{V_{o1}+Ax}\dot{m}_1 + \frac{\dot{Q}(k-1)}{V_{o1}+Ax} \quad (10)$$

The third term to the right-hand side of Eq. 10 models the effect of head losses along the chamber. Its practical implementation for all operation circumstances is rather difficult because it implies the knowledge of the velocity of air along the pipe, which is not easily accessible in the real plant. Additionally, it becomes necessary to increase the order of the dynamical system. For these reasons, instead of directly integrating this term, the head losses are taken into account only in the main ducts, and their effects are assumed to be satisfactorily approximated by means of a classic steady-state approach described in Fox and McDonald (2006), valid for low pressures such as those found in the Aeromovel system. According to the aforementioned authors, the head losses caused by a fluid moving with average velocity $\bar{v}$ along a pipe with length L_0 and equivalent diameter D are given by $h_{lt} = fL_0\bar{v}^2/(2D)$, where f is the friction factor for turbulent flows. In this work, the air velocity is regarded in terms of the velocity of the vehicle as it moves along the line. This approach is justified because the low amplitudes the steady-state pressures cause the flow along the pipes to be nearly incompressible. Thus, the air flows inside the chambers are approximately equal to the rate at which their volumes vary, which is proportional to the velocity of the vehicle. Thus, after integrating the first two right-hand side terms of Eq. 10, the head losses term is directly added to the resulting function, being represented as a difference between the pressure in the flow entrance (e.g. region of the chamber close to the propelling unit) and the one that is actually applied to the piston of the vehicle (refer to Figures 2 and 4). By going through this procedure, the dynamics of the pressures on the piston surface are described by Eqs. 11 and 12:

$$p_1 = p_{1al} + f\frac{x}{D}\frac{\dot{x}^2}{2}\frac{p_{1al}}{RT} \quad (11)$$

$$\frac{dp_{1al}}{dt} = -\frac{p_{1al}kA}{V_{o1}+Ax}\dot{x} + \frac{RkT}{V_{o1}+Ax}\dot{m}_1 \quad (12)$$

Similarly, for control volume 2, at the downstream side, the pressure dynamics can be written as:

$$p_2 = p_{2al} - f\frac{(L-x)}{D}\frac{\dot{x}^2}{2}\frac{p_{2al}}{RT} \quad (13)$$

$$\frac{dp_{2al}}{dt} = \frac{p_{2al}kA}{V_{o2}+A(L-x)}\dot{x} + \frac{RkT}{V_{o2}+A(L-x)}\dot{m}_2 \quad (14)$$

where L is the distance between stations. The air mass flows $\dot{m}_1$ and $\dot{m}_2$ required for evaluating Eqs. 12 and 14 result from a number of auxiliary mass flow terms, which are defined in Sections 3.3–3.5.

3.3. PPU

A regular PPU is presented in Figure 5. When in Push mode, valves 1 and 4 are open and valves 2 and 3 are closed. In the Pull configuration, this order is reversed.

Applying once more the energy conservation principle, the time derivatives of the pressures inside of each volume referred to station 1 can be written as:

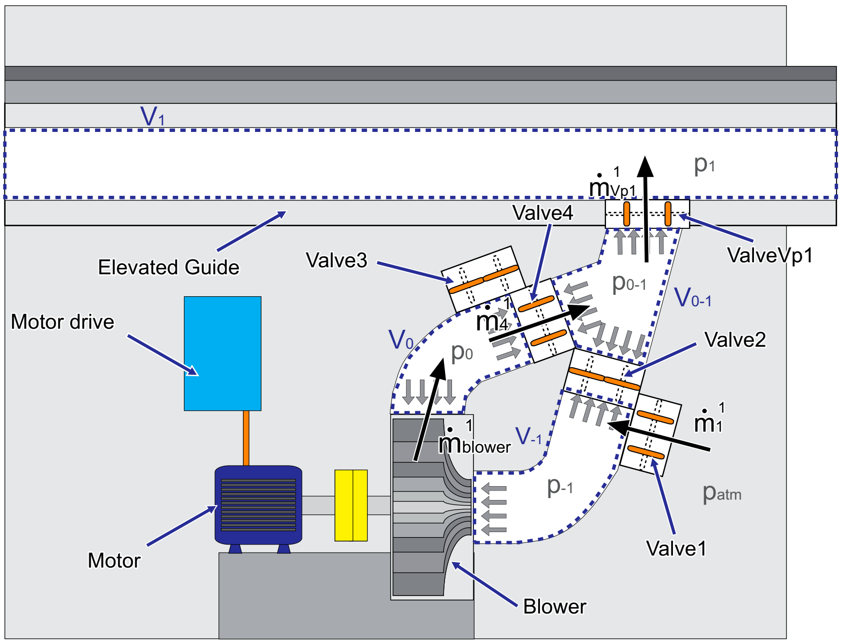

Figure 5. Scheme of a PPU.

$$\frac{dp_0^1}{dt} = \frac{RkT}{V_0^1}\left(\dot{m}_{blower}^1 - \dot{m}_3^1 - \dot{m}_4^1\right) \quad (15)$$

$$\frac{dp_{-1}^1}{dt} = \frac{RkT}{V_{-1}^1}\left(\dot{m}_1^1 + \dot{m}_2^1 - \dot{m}_{blower}^1\right) \quad (16)$$

$$\frac{dp_{0-1}^1}{dt} = \frac{RkT}{V_{0-1}^1}\left(\dot{m}_4^1 - \dot{m}_2^1 - \dot{m}_{Vp1}^1\right) \quad (17)$$

where $\dot{m}_{blower}^1$ is the air mass flow through the blower; p_0^1 and p_{-1}^1 are, respectively, the downstream and upstream pressures on the blower; p_{0-1}^1 is the pressure between the valves 2, 4 and V_{p1}; $\dot{m}_1^1$, $\dot{m}_2^1$, $\dot{m}_3^1$, $\dot{m}_4^1$ are the air mass flows rates through the respective PPU valves, $\dot{m}_{Vp1}^1$ is the air mass flow through V_{p1}; and V_p^1, V_0^1, V_{-1}^1, V_{0-1}^1 are the control volumes. The calculations of each of the aforementioned air mass flows are described in Sections 3.3.1 and 3.3.2.

3.3.1. *Blower model*

A centrifugal backward-curved-blade fan is used at the experimental line, and its modelling is based on the empiric static characteristic curves supplied by its manufacturer. By employing the *fan laws* (Henn, 2001), these curves can be generalised for different values of angular speed and density of air. The curves of the air mass flow rate as a function of pressures and of the motor angular speed, adapted from the manufacturer data sheet by using least-squares fitting, can be expressed by:

$$\dot{m}_{blower} = \frac{\rho_d}{\rho_{blow}}\dot{m}_{\max}\frac{\omega_{blower}}{\omega_{blower\max}}\left(0,2523 + \sqrt{0,5618 - 0,5556\frac{(p_d - p_{atm})\rho_{blower}(\omega_{blower\max})^2}{(\omega_{blower})^2 p_{man\max}\rho_d}}\right) \quad (18)$$

where ω_{blower} and $\omega_{blower\max}$ are, respectively, the angular velocity of the blower and its corresponding maximum value; $\dot{m}_{\max}$ and $p_{man\max}$ are the maximum air mass flow rate and the maximum downstream pressure that can be achieved by the blower; ρ_d is the downstream air density; and ρ_{blow} is the air density at which the characteristic curve was determined. This air mass flow is taken into account in the whole PPU model by substituting the value obtained in Eq. 18 into Eqs. 15–17.

3.3.2. *Control valves model*

All valves in the PPU are of butterfly type, driven by pneumatic pistons which regulate their air passage apertures by means of angular movements. Their typical geometric configuration is depicted in Figure 6(a), where an atmospheric valve is presented. In Figure 6(b), it is shown how the air mass flow rates through these valves depend on their opening angles and on their upstream and downstream pressures. This relationship was evaluated by means of approximate correlations for constricted flow regimes, as described in Susin (2008).

The air mass flows through all control valves are assumed to conform to the empiric expression proposed by Boulter (1999):

$$\dot{m}_n = K_{qm}u_{val}\sqrt{\max(p_u, p_d) - \min(p_u, p_d)}\,\mathrm{sgn}(p_u - p_d) \quad (19)$$

where the sub-index n identifies each valve; p_u and p_d denote, respectively, the upstream and downstream pressures; K_{qm} is an associated mass flow rate gain and u_{val} is the input control signal. Eq. 19 represents the surface presented in Figure 6(b).

3.4. **Air leakages model**

The proposed model represents two types of leakages: (i) from the pipe chambers to the atmosphere due to the coupling of the line piston to the vehicle, represented in Figure 2 by the terms $\dot{m}_{atm1}$ and $\dot{m}_{atm2}$; (ii) from one adjacent pipe chamber to another due to the area differences between the cross-section of the pipe and the sealing surfaces of the line pistons, also depicted in Figure 2 by $\dot{m}_{1.12}$ and $\dot{m}_{2.12}$. The modelling of all of these leakages is based on the description of the constricted flow of a compressible fluid (Fox and McDonald, 2006). For a general orifice with area A_o, submitted to adjacent upstream and downstream pressures given respectively by p_d and p_u, the general form for such expressions is:

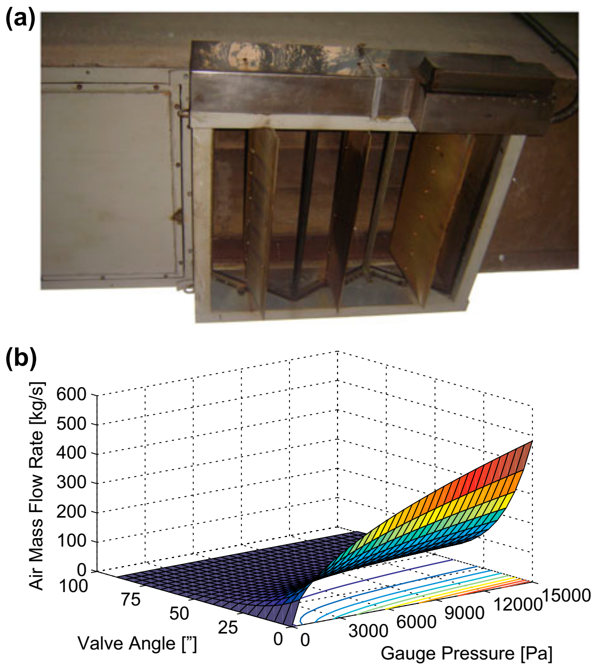

Figure 6. Flow control valve. (a) Atmospheric valve (dimensions 1 m × 1 m), (b) Air mass flow rates through the valves.

$$\dot{m} = A_o \sqrt{\frac{2k}{RT(k-1)}} \max(p_d, p_u) \mathrm{sgn}(p_d - p_u) \sqrt{\left(\frac{\min(p_d,p_u)}{\max(p_d,p_u)}\right)^{\frac{2}{k}} - \left(\frac{\min(p_d,p_u)}{\max(p_d,p_u)}\right)^{\frac{k+1}{k}}} \quad (20)$$

For leakages between adjacent chambers, the orifice area is given by the geometric difference A_{leak} between the cross-sectional areas of the pipe and the sealing surfaces of the pistons. The areas related to the leakages from the pipe chambers to the atmosphere vary with the position x of the vehicle, depending on the length of each chamber and the width esp_{seal} of the gap between the sealing blades. Thus, for chambers 1 and 2, respectively, this area is given by $esp_{seal}x$ and $esp_{seal}(L - x)$.

3.5. Model integration

In order to integrate the equations developed in the previous sections and complete the model, it is necessary to use all the auxiliary terms defined in Sections 3.3 and 3.4 to evaluate the air mass flows $\dot{m}_1$ and $\dot{m}_2$ required in Eqs. 12 and 14. These expressions can be obtained by summing the effects of the volume variations of each chamber, the mass flow rates provided by the blower, the leakages, and the exhausting effects:

$$\dot{m}_1 = \dot{m}_{Vp1} - \dot{m}_{Va1} - \dot{m}_{1.12} - \dot{m}_{atm1} \quad (21)$$

$$\dot{m}_2 = \dot{m}_{Vp2} - \dot{m}_{Va2} + \dot{m}_{2.12} - \dot{m}_{atm2} \quad (22)$$

where $\dot{m}_{Va1}$ and $\dot{m}_{Va2}$ are the mass flow rates related to the atmosphere valves 1 and 2. Their values are determined in the same way described in Section 3.3.2.

Finally, in terms of the more general phenomena involved in its operation, Eqs. 1–7 and 9–22 constitute the complete mathematical model proposed for the Aeromovel system.

4. Test line

This section is dedicated to describe the dimensions and characteristics of the test line, whose partial view is presented in Figure 7. Figure 8 illustrates the entire line, complemented with a schematic view of its structure.

Due to economic constraints, the test line is designed as a simplified shuttle arrangement, operating with only one PPU, as shown in Figure 8. In theory, other operational configurations can also be made available, allowing multiple vehicles to run concurrently in the same line and in different directions (see Kunz et al., 2011b). The proposed model is based on the system described in Section 2, which is suitable for a "complete" shuttle application. However, as the main elements of the Aeromovel system are always the same, this model can be applied to any of its line configurations, provided that the appropriate modifications are made in the number and positions of the PPUs and in the activation sequence of their corresponding control valves.

4.1. Dimensions

The line has a total extension of about 958 m, with two stations 655 m apart from each other. One portion of the line is curved, with radius of 156 m. The station *Fazenda* and the main line were built at a distance of 5.5m from the soil level. The other station, *Gasômetro*, is elevated 6.5 m above the soil. The part of the line that

Figure 7. Test line in Porto Alegre, Brazil.

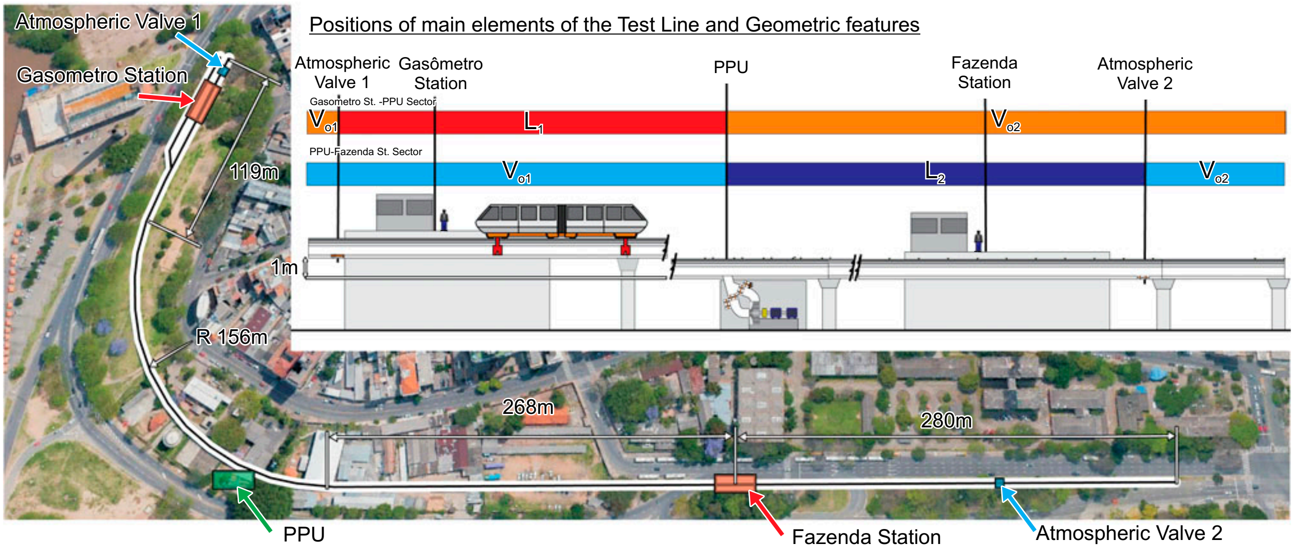

Figure 8. Test line (image by Google Earth, 2013) with schematic description.

links the *Gasômetro* station to the main line has an inclination of approximately 3º. Near this station, there is a bifurcation on the line used for removing vehicles from the main line for maintenance procedures. The distance between PPU and V_{a2} is about 344 m, while the PPU and V_{a1} are about 495 m apart.

4.2. Operation

In the experiments, the system was evaluated in terms of its open-loop step response, which is a common test condition when control applications are considered. Therefore, each test starts with the PPU fan already operating at a constant velocity of 126 rad/s and with the atmospheric valve corresponding to the desired direction of movement entirely open when V_{p1} is suddenly opened to its maximum value of 1 m^2. Then, the valves are kept completely open until the vehicle approaches the next section of the line. For instance, in a standard round trip starting from *Gasômetro* station, V_{a1} and V_{p1} are initially kept open so that the PPU exhausts the pipe inside the line, causing the vehicle to leave the station and move until it reaches the PPU region. Then, with V_{p1} still open, the PPU control valves invert the direction of the air flow, V_{a1} is closed and V_{a2} is opened. As a consequence, the pipe is pressurised, pushing the vehicle towards *Fazenda* station. At a distance of 90 m from this station, V_{p1} is closed and the brake control system is activated so that the vehicle stops. The return trip occurs by means of a similar procedure, with the order of activation of the atmospheric valves being suitably inverted.

4.3. Dead volumes

As the PPU is located between the stations, the whole pipe must be fully exhausted or pressurised on each journey. Thus, it is convenient to analyse the operation of the vehicle in terms of two different sectors, delimited by the parts of the line between the PPU and the atmospheric valves close to each station. So, the sector *Gasômetro* (with dead volume V_{o1}) corresponds to the part between V_{a1} and the PPU, whereas the sector *Fazenda* (with dead volume V_{o2}) corresponds to the part between the PPU and V_{a2}. Therefore, the remaining parts of each sector are interpreted by the computational model as *dead volumes* calculated by the multiplication of their lengths by the cross-sectional area of the pipe.

Because of the asymmetries in the configuration of the system, depending on the direction of the travel (*Gasômetro* towards *Fazenda* – GF, or *Fazenda* towards *Gasômetro* – FG), different dead volumes are achieved. Additionally, the dead volume due to the maintenance line (V_{odesv}) must also be taken into account.

5. Model evaluation

This section compares the simulation results with experimental data in terms of the pressures in the pipe chambers and of the acceleration, velocity, and position of the vehicle. The simulations were performed using a Matlab/Simulink package processing Runge–Kutta integration method with step of 1×10^{-3} s.

The values of all parameters are listed in the nomenclature at the end of this work. Most of them were acquired experimentally or from catalogue information provided by the corresponding manufacturers. The equivalent Coulomb force coefficient of the seals F_{seal} varies depending on the movement direction. Therefore, it is considered by means of two different values (F_{seal11} or F_{seal12}, associated, respectively, to GF or FG cases). Some parameters were estimated by means of approximations commonly employed in the specialised literature. For instance, the specific heat constants ratio k for air was assumed to be $k = 1.4$, based on the case of small-scale pneumatic actuators (Virvalo and Koskinen, 1988, Maré et al., 2000), in which the thermodynamical processes in the chambers are usually considered as adiabatic and reversible (isotropic). The friction factor, *f*, which is dependent on the Reynolds number and the pipe-wall roughness, was estimated by using standard values for air parameters and a very conservative value of 1.84×10^{-5} [Ns/m] for the flow medium velocity. Under such conditions, the corresponding Reynolds number is 2300, indicating a turbulent flow. Taking an estimated wall-roughness value of 0.15 mm, a recursive calculation of the Colebrook equation (Fox and MacDonald, 2006) shows that f results between 0.015 and 0.022. For the operational velocities of the Aeromovel system, this value tends to $f \cong 0.015$, which is adopted in this work.

The vehicle is equipped with magnetic-pulse speed sensors with input resolution 3.2 cm, which operate in the same way as an optical incremental encoder, allowing velocity and displacement data to be acquired directly. The actual position is estimated by integrating the signal from the velocity sensors. Similarly, the acceleration values were obtained through numerical differentiation of the measured velocity. Both numerical estimates were determined by means of the standard forward finite-difference method. The pressures applied to the pistons were measured by membrane sensors connected to their external surfaces, i.e. on the surfaces that are submitted to pressures p_{1al} and p_{2al} as depicted in Figure 2. More information about the measurement apparatus, such as the technical specifications of the analogue-to-digital interface of the system, can be found in Britto (2008).

In Figures 9–11, the predictions made by means of the proposed model are compared to experimental results collected during a typical round trip. The vehicle departs from *Gasômetro* station towards *Fazenda* station (GF), and, after a brief stopping, makes the reverse trip (FG). During the trip, it carries 97 barrels filled with water to emulate the effect of passenger loading, resulting in a total mass is of 10.922 kg. The signs of the kinematic variables are inverted when the vehicle starts its returning trip, so that all velocities are positive and the distance travelled can be accessed in a cumulative form.

In Figure 9, the results regarding the pressures inside the line chambers are presented. Along the trajectory, these pressures vary due to several factors, such as vehicle movement, leakages, status-changing of the atmosphere valves, head losses, braking action, and different PPU configurations. The biggest difference between simulation and experiment occurs when, in the GF travel, the inversion of the PPU action is performed ($t \cong 50\,s$), changing from pull to push operation mode. At this point, diversely from simulations, experimental data show the occurrence of a pressure peak in both chambers. This is probably due to synchronism problems between the PPU actuation and the vehicle position on the plant, caused by differences in the time response of

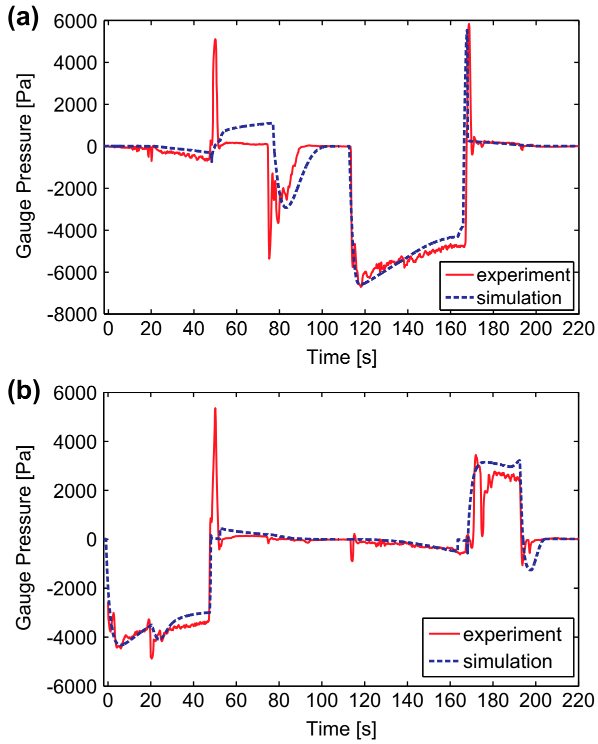

Figure 9. Experimental and simulation results: pressures in the chambers. (a) Pressure in Chamber 1, (b) Pressure in Chamber 2.

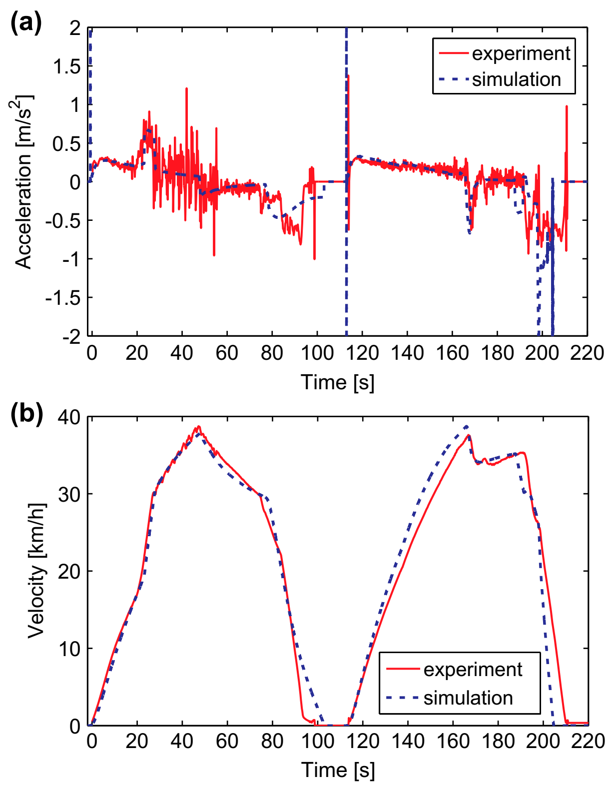

Figure 10. Experimental and simulation results: acceleration and velocity of the vehicle. (a) Acceleration, (b) Velocity.

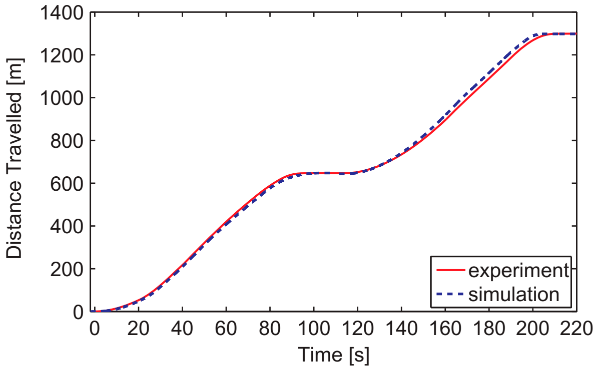

Figure 11. Experimental and simulation results: distance travelled.

the flow-directional valves that were not considered in the model.

The evaluation of the model regarding acceleration and velocity data is presented in Figure 10. The results indicate that, in spite of the noise existing on the measured signal, the predictions agree with the experiment. In particular, it should be noticed that the acceleration values (Figure 10(a)) are satisfactorily verified when the vehicle passes on the raising ramp in the line (about $t = 23$ s), and when it crosses the PPU region ($t = 47$ s and $t = 167$ s), situations that are characterised by sudden and sharp variations in the operation conditions of the system.

In Figure 10(b), it is shown that simulation results underestimate the velocity on the advance travel, whereas its corresponding value on the return travel is overestimated. Experimental investigation carried out in the test line indicated that this difference is probably related to the large variations in the behaviour of the pipes sealing elements along the line, which cause diverse levels of leakages and of resistive forces on different parts of the trajectory. Finally, in Figure 11, it can be observed that the simulation results for the cumulative distance travelled by the vehicle along time present small deviations when compared to the measured data.

6. Conclusion and future work

The comparison between simulation and experimental data results has shown satisfactorily small deviations between the measured variables and their predicted values, which allows concluding that the proposed mathematical model can be used in the analysis and design of new applications of the Aeromovel technology.

Future work will focus on refining the model in those points where its predictions are not yet satisfactorily accurate, as in the case of the role played by the pipe seals. As the system operates currently with a constant fan speed and with constant valve openings, future work will also include the use of the model in studies aiming to improve both its energetic efficiency and dynamic performance by the combined control of the angular velocity of the blower and of the opening of the valves. Thus, in order to represent the energetic losses of the system in a more complete way, the modelling of both transient and steady-state effects of the head losses in the PPU and in the control valves will also be addressed.

Nomenclature

a	half axis of the contact ellipse 0.0028 m
A	pipe area 1 m^2
A_{al}	piston area 0.98 m^2
A_{br}	brake piston contact area 0.0002 m^2
A_{eq}	vehicle transversal section area 0.98 m^2
A_{leak}	piston leakage area 0.005 m
b	half axis of the contact ellipse 0.0017 m
B_{seal}	seal Newton friction coefficient 10 Ns/m
c_{11}	Kalker coefficient 4853
c_D	drag coefficient 1/5 Ns^2
c_p	specific heat at constant pressure [J/kgK]
c_v	specific heat at constant volume [J/kgK]
c_{wh}	angular viscous friction constant 0.005 Nms/rad
e	specific energy [J/kg]
E	energy [J]
esp_{seal}	seal piston rod gap 3.10^{-5} m
f	friction factor for turbulent flows 0.015
G	shear module 8.27×10^{10} N
F	force [N]
F_{seal11}	dry friction of piston 1 (GF) 476 N
g	gravity acceleration [m/s^2]
J_{wh}	moment of inertia of the wheels 10.4 kg/m^2
k	specific heat constants ratio 1.4
K_{qm}	valve constant 0.026 kg/sPa$^{1/2}$
L	distance [m]
L_1	distance between PPU and V_{a2} 345 m
L_2	distance between PPU and V_{a1} 495 m
m	mass [kg]
m_{vehic}	empty vehicle mass 5620 kg
$\dot{m}$	mass flow rate [kg/s]
p	pressure [Pa]
p_{atm}	atmosphere pressure 101325 Pa
p_{brake}	brake pressure 9.4 MPa
$\dot{Q}$	heat transfer rate [J/s]
R	gas constant 286.9 J/kgK
r_{br}	brake calliper radius 0.115 m
r_{cv}	curvature radius of the line [m]
r_{wh}	wheels radius 0.25 m
S	surface [m^2]
$Slip$	creep in the longitudinal direction
T	temperature 293.2 K
Γ	torque [Nm]
u_i	specific energy [J/kg]
u_{val}	control signal
v	velocity [m/s]
V	volume [m^3]
V_{o1} (GF)	upstream volume Gasômetro part 4.25 m^3
V_{o2} (GF)	downstream volume Fazenda part 609 m^3

V_{o1} (FG)	upstream volume Gasômetro part 349 m^3
V_{o2} (FG)	downstream volume Fazenda part 114 m^3
V_{odesv}	volume of maintenance part 88 m^3
$\dot{V}$	volumetric flow rate [m^3/s]
x	vehicle position [m]
W_{wh}	weight held by each wheel 1.365 kg
z	height coordinate [m]
ε	gradient of tangential stress
ϕ_z	slope angle. [rad]
μ	wheel-rail friction coefficient 0.025
μ_{diskE}	dry brake friction coefficient 0.4
μ_{diskV}	viscous brake friction coefficient 0.003 s/rad
θ	angular displacement [rad]
ρ_{air}	air density 1.2 kg/m^3
σ	normal stress [N/m^2]
τ	tangential stress [N/m^2]
ω	angular velocity [rad/s]

Notes on Contributors

João F. F. H. Britto is a Mechanical Engineer at the E&P Production Development Projects – Artificial Lift and Subsea Dept. Petrobrás, Rio de Janeiro, Brazil. In 2008, he obtained his M.Sc. Degree in Mechanical Engineering from the Universidade Federal do Rio Grande do Sul (Brazil). His work includes conceptual and basic design, and operational and maintenance of O&G subsea production systems. His research interests include design, modelling, simulation, analysis, and control of mechanical systems.

Eduardo A. Perondi is a Professor at the Mechanical Engineering Department of Universidade Federal do Rio Grande do Sul, Brazil, and coordinator of the LAMECC – Laboratory of Mechatronics and Control at the same university. In 2002, he obtained his Ph.D. in Mechanical Engineering from the Federal University of Santa Catarina (Brazil). His research and teaching interests include design, modelling, simulation, analysis, and control of mechanical systems.

Mário R. Sobczyk S. is a Professor at the Mechanical Engineering Department of Universidade Federal do Rio Grande do Sul (UFRGS), Brazil, where he obtained his Ph.D. in Mechanical Engineering in 2009. He is a researcher at the Laboratory of Mechatronics and Control (LAMECC) of the same university. His research and teaching interests include modelling, simulation, analysis, and control of mechanical, fluid-mechanical, and electromechanical systems.

References

Aeromovel. 2013. Retrieved from www.aeromovel.com.br

Boulter, B. T. 1999. Aeromovel Vehicle Speed Control System Analysis. *Rockwell Automation Reliance Electric* Pub. Greenville, Brazil.

Britto, J. F. F. H. 2008. *Modelo Computacional do Sistema Aeromóvel de Transportes*. M.S. thesis, UFRGS, Porto Alegre, Brazil.

Costa, E. C. 1981. *Parecer técnico sobre o sistema de transporte pneumático Coester Aeromóvel*. Technical Report (http://www.coester.com.br/). Porto Alegre, Brazil.

Ferreira, V. 1984. Análise simulada do sistema de propulsão - Relatório Parcial. *Fundatec*. Porto Alegre, Brazil (http://www.fundatec.org.br/).

Ferreira, V. and Sadhu, D. P. 1981. *Aeromóvel: Avaliação do Desempenho Técnico e Competitividade*. Fundatec. Porto Alegre, RS, Brazil (http://www.fundatec.org.br/).

Fox, R. W. and McDonald, A. T., 2006. *Introduction to Fluid Mechanics*. John Wiley, Hoboken, NJ.

Freitag, J. and Detoni, J., 2000. *Caderno de Especificação Técnica – Frenagem do Aeromóvel*. Eletrix Technical Report. Porto Alegre, Brazil.

Henn, E. L. 2001. *Fluid Machines*. Ed. UFSM, Santa Maria, Brazil.

Kalker, J. J. 1982. A Fast Algorithm for the Simplified Theory of Rolling Contact, Vehicle System Dynamics: International *Journal of Vehicle Mechanics and Mobility*, Vol. 11, No. 1, pp. 1–13.

Kunz, G. O., Perondi, E. A. and Machado, J. M. 2011a. Modelling and Simulating the Controller Behaviour of an Automated People Mover using IEC 61850 Communication Requirements. *Proceedings of 9th INDIN*, Lisbon, Portugal.

Kunz, G. O., Perondi, E. A. and Machado, J. M. 2011b. Modelling and Simulation of IEC 61850 Requirements Applied to an Automated People Movers Controller. *Proceedings of 8th ICINCO*, Noordwijkerhout, The Netherlands.

Maré, J.-C., Geider, O. and Colin, S., 2000. An Improved Dynamic Model of Pneumatic Actuators. *International Journal of Fluid Power*, Vol. I, No. (2), pp. 39–47.

Perondi, E. A. and Guenther, R. 2000. Control of a Servopneumatic Drive with Friction Compensation. *Proceedings of 1st FPNI PhD Symposium*, Hamburg, Germany.

Polach, O., 2005. Creep Forces in Simulations of Traction Vehicles Running on Adhesion Limit. *Wear*, Vol. 258, pp. 992–1000.

Sarmanho, C. A., Perondi, E. A., Sobczyk, S. and M. R. 2011. Gain-Schedule Control Based on Mass Estimation Applied to the Braking System of an Urban Automated People Mover. *Proceedings of 21st COBEM*, Natal, Brazil.

Sobczyk, S. M. R., Britto, J. F. F. H. and Perondi, E. A. 2008a. Cascade Nonlinear Control of Pneumatic Actuators Applied to the Aeromovel Transport System. *Proceedings of 5th FPNI PhD Symposium*, Cracow, Poland.

Sobczyk, S. M. R., Perondi, E. A. and Britto, J. F. F. H. 2008b. Nonlinear Cascade Control Applied to a Pneumatic Urban Transport System. *Proceedings of 8th CONTROLO*, Vila Real, Portugal.

Susin, M. P. B. 2008. *Análise Numérica da Válvula Atmosférica – Projeto Aeromóvel*. B.Sc. Thesis. UFRGS, Porto Alegre, Brazil (http://sabi.ufrgs.br).

Virvalo, T. and Koskinen, H., 1988. Electro-pneumatic Servo System Design. *Fluid Power International*, Vol. 34, pp. 141–147.